Tunable Plasmonic Nanogap Resonators

Tiziana C. Bond, Mihail Bora, Allan S.-P. Chang,
Center of Micron and Nano Technology
Lawrence Livermore National Laboratory
Livermore, USA
e-mail: bond7@llnl.gov, bora1@llnl.gov, chang@llnl.gov

***Abstract*—We present a new class of plasmonic substrates based on two-dimensional rectangular array of nanopillars over very large areas (4" wafers). The gap between each pair of neighboring nanopillars is small enough (< 100 nm) that highly confined plasmonic cavity resonances are supported in between such pairs. The resonant structures are tunable in the 400-800nm visible range with strong field enhancements and antireflective performance, up to 80% of incident light due to a highly efficient coupling and trapping. Because of their design and fabrication flexibility, these nanotemplates they can impact various fields, from detection and spectroscopy to energy harvesting to photovoltaic.**

Keywords- plasmonics; resonant cavity; tunability; nanolithography.

I. INTRODUCTION

Plasmonic nanostructures are widely investigated due to their strong controllability potential which suite their exploitation in disparate fields from bio-molecular detection [1-3] to sub-wavelength optics [4-6] and photovoltaic technology [7-9]. A plethora of 2D particle geometries have been employed but typically offer enhancements over narrow wavelength and incident angle ranges [10, 11]. There are currently new efforts in overcoming this inherent limitation of plasmonic nanostructures exploring also the third dimension [12-15]. Here, we propose a controllable broadband, tunable platform in which vertical plasmon resonant nanocavities are arranged in uniform and dense arrays of coupled metallic nanowires [16]. Tuning and broadening of the plasmonic multiple resonances is obtained by controlling the geometrical dimensions of the cavity, i.e interpillar gaps and heights, or the optical properties of the environment, i.e., the dielectric constant. In particular, the vertical dimension dictates the total number of supported wavelength resonances, whereas the horizontal dimension is responsible for the quality factor Q of the cavities. Using such knobs, UV to IR spectrum could be covered at once with less or more resonant plasmonic features favoring the conditions for either specific wavelength alignment with high Q as needed in spectroscopy or widely absorbing plasmons more critical in energy harvesting applications. Furthermore, because of the square lattice arrangement of the pillars, the platform is also polarization independent which can be advantageous as it reduces requirements of the available sources (i.e., Light Emitting Diodes or LEDs). In the following we will discuss about the technology providing high density tunable plasmonic paired nanopillars with excellent control of the cavity size over 4" wafers. Tuning of the plasmon resonance in the 400-800 nm range is demonstrated by controlling the geometrical dimensions of the cavity and the dielectric environment. The reflectivity and absorbance of the arrays of cavities for gold, silver and aluminum metals are presented. The limitations for the implementation of such a structure are discussed nevertheless showing that the averaged absorbance can be increased above 80%, a remarkable feature considering that these metals are used to fabricate highly reflective optical mirrors.

The paper is structured as follows: we will provide first a description of the experimental work, including the fabrication details, the principle of operation, the characterization setup , along with data derivation and model validation. Discussion of the results will follow. Finally, the conclusion and future outlook are presented.

II. EXPERIMENTS

A. Fabrication of Nanopillr Templates

The plasmonic substrate is composed of a rectangular array of vertical nanopillars coated with either gold, silver or he fabrication steps are reported in Fig. 1

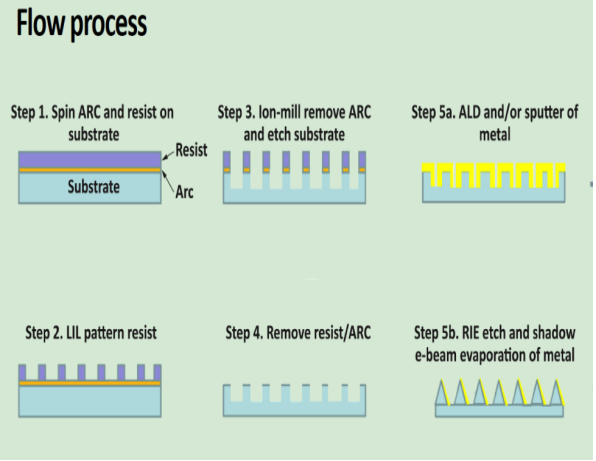

Figure 1. Fabrication steps details.

The period of the array is 360 nm, chosen such that insignificant diffraction grating effects take place in the visible spectrum. The nanopillar array template is patterned

 ISBN: 978-1-61208-214-1

using laser interference lithography [17] over 4" wafers that are coated with half-micron thick photoresist. The laser wavelength for the holography is 413 nm and the dose ~ 40 mJ/cm^2. The resultant photoresist structure is a periodic array of pillars with pitch of 360 nm and diameter ranging between 130 - 150 nm due to source dose variation. The patterned photoresist acts as the etching mask in a subsequent step of ion beam milling which enables the transfer of the geometry into a silicon or fused silica substrate. Further, the structure is either sputtered with conformal metallic films or coated first with a thick layer of Al_2O_3 by Atomic Layer Deposition (ALD) followed by a subsequent step of conformal sputtering of thinner metal layers. In this context we will discuss only the results obtained with the former as it gives more flexibility in controlling the aspect ratio of height vs. gap (or diameter of the pillars) due to the different vertical vs. sidewall deposition rates, eventually resulting more amenable to achieve the desired tunability. In fact, the height and diameter of the pillars are determined by the etch time and sputtering time respectively as shown in Figs. 2a and 2b. Incidentally, the combined ALD/sputtering process becomes more appealing for applications that require much smaller gaps (< 10 nm) such as Surface Enhanced Raman Spectroscopy, as it helps in refining the dimensions at the atomic level [18]. Pairs of vertically aligned nanopillars form a metal-dielectric-metal (MDM) waveguide when the edge to edge separation is closer than 100 nm (Fig. 2c). Plasmon modes are excited by normal incident light waves in the transverse magnetic (TM) polarization mode as exemplary polarization; for the transverse electric (TE) results would be just the same given the lattice symmetry.

B. Plasmonic Resonance Cavity Model

The resonant modes of the cavity are formed by the interference of forward and backward propagating waves and are determined by the dispersion relation of the waveguide and the phase shifts at each end

$$2k_{sp}h + \varphi_1 + \varphi_2 = 2m\pi, \quad (1)$$

where k_{sp} is the wavevector of the surface plasmon wave, h is the length of the cavity, φ_1 and φ_2, are the phase changes at the top and bottom boundaries and m is the resonance order. The dispersion relation, $k_{sp}(\omega)$ can be approximated with that of a semi-infinite planar MDM waveguide or calculated nuemrically. Fig. 2d shows the electric field amplitude profile for a resonant mode of order m = 4, as seen from three orthogonal cross sections. The node and anti-node conditions at each end are assumed to correspond to phase shifts of *0* (matched dielectric) and *π/2* (metal interface). In Fig. 2e we highlight the tangential power flow for the m = 4 mode. A net power flow occurs in the horizontal directions only at the rounded tapered region corresponding to a lateral flow convergent into the inter-wire waveguide. The curved ending acts as a sub-wavelength electromagnetic antenna that effectively increases the absorbance cross section of the cavity.

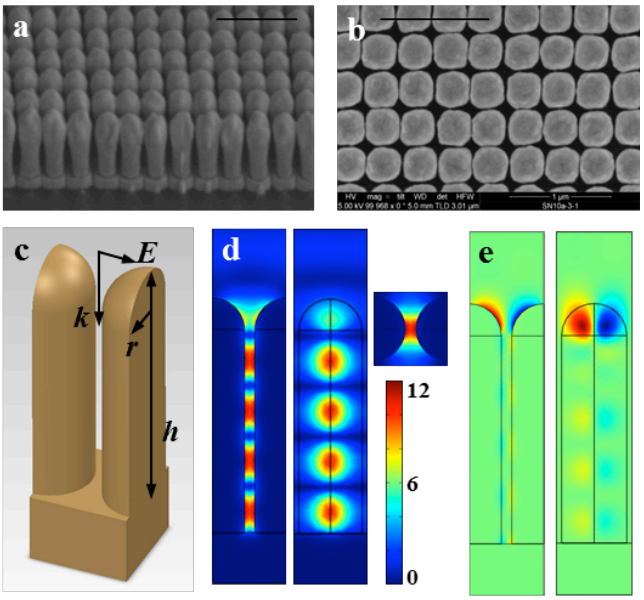

Figure 2. Fabrication: SEMs of the vertical metallic nanopillars viewed from side (a) and top (b); bar = 1 μm. Simulation: (c) Unit cell of the rectangular array centered on the plasmon nanocavity. (d) Electric field amplitude in the resonator seen from front, side and top when excited by noramlly incident TM mode. (e) Power flow in the vertical symmetry planes of the cavity channeled into the inter-pillar region from the top of the cavity.

C. Characterization and Model Validation

The frequency response of the resonator shows strong absorbance peaks that correspond to excitation of high electric field amplitude modes. The overall absorbance can be increased by adjusting the length of the resonator such that additional higher order modes are excited. Fig. 3 represents the simulated and experimentally measured reflectance of an array with 360 nm pitch made of silver nanopillars of 310 nm diameter and 1000 nm height. The electric field amplitude profile of the mode on the vertical symmetry axis of the unit cell is plotted as a function of wavelength. The plasmon cavity shows the strongest field enhancements for the modes that extend further into the free space and have a better overlap with the incident photon field. However, weak plasmon modes at other wavelengths, suggesting that stronger absorbance of the array over the whole spectrum can be achieved by engineering the ends. The directionality of the antenna is shown in Fig. 3c.

Array reflectivities were calculated for nanopillar arrays of variable height made of gold, silver and aluminum which arranged in the increasing order of their bulk plasma frequency [19]. The gold is significant for bio-molecular sensing, while silver and aluminum are relevant for photovoltaic applications since resonances have a better overlap with the solar spectrum.

In Fig. 4 we show the simulated reflectance spectrum of 360 nm pitch array of vertical nanowires of diameter 310

 ISBN: 978-1-61208-214-1

nm, variable height *h*, and capped by a hemisphere of diameter 310 nm. In the case of gold only a fraction of the visible spectrum is covered by plasmon resonances as the cut off frequency corresponds to an excitation wavelength of 550 nm, while for silver and aluminum the entire visible spectrum is covered. As the height of the pillar is increased the spacing between consecutive modes is decreasing enabling the cavity to have a strong absorbance at more excitation wavelengths. The simulations for the aluminum structures suggest that past a certain height, an increase in the length of the resonator causes a decrease in the absorbance strength. This can be explained by the higher losses of aluminum combined with longer paths of the plasmon at the interfaces. Alternatively, the effective length of the resonator can be changed by increasing the refractive index of the dielectric core as shown in Fig. 4g.

The effectiveness of the resonant array as a broadband absorber was assessed by calculating the average absorbance of the array in the 400-800 nm spectral range as a function of nanopillar height (Fig. 5). A stepwise decrease in absorbance is observed each time an additional resonance is added to the reflectance spectrum of the array.

The averaged absorbance becomes larger than the values calculated in Fig. 5 when restricted to a frequency range above common semiconductor bandgaps and when weighted by the photon energy and the solar irradiance spectrum. If the refractive index of the inter-pillar dielectric core is increased, the cutoff plasma frequency and the plasmon resonance locations are red shifted and the spacing between resonances becomes smaller as the optical length of resonator is increased. Based on these arguments, aluminum nanopillar dielectric hybrid structures have a better spectral coverage than any other metal considered. Silver on the other hand has the lowest losses in the visible and it is most efficient for transferring energy from the plasmon modes into

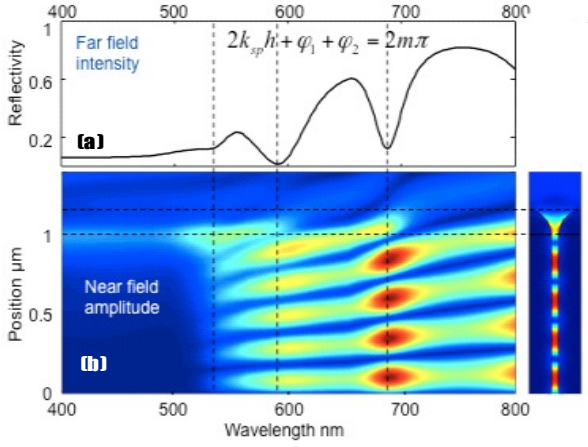

Figure 3. (a) Normal incidence reflectance (simulation and experiment) for a gold nanocavity 1000 nm long, 60 nm wide, showing full resonances of order 4, and 5. (b) Electric field amplitude of the plasmon mode in the center of the cavity plotted as a function of position and excitation wavelength. (c) Radar mapping showing directionality of the nanopillar antennae.

the absorptive dielectric material. The gold nanowire arrays have a significant potential for biological sensing.

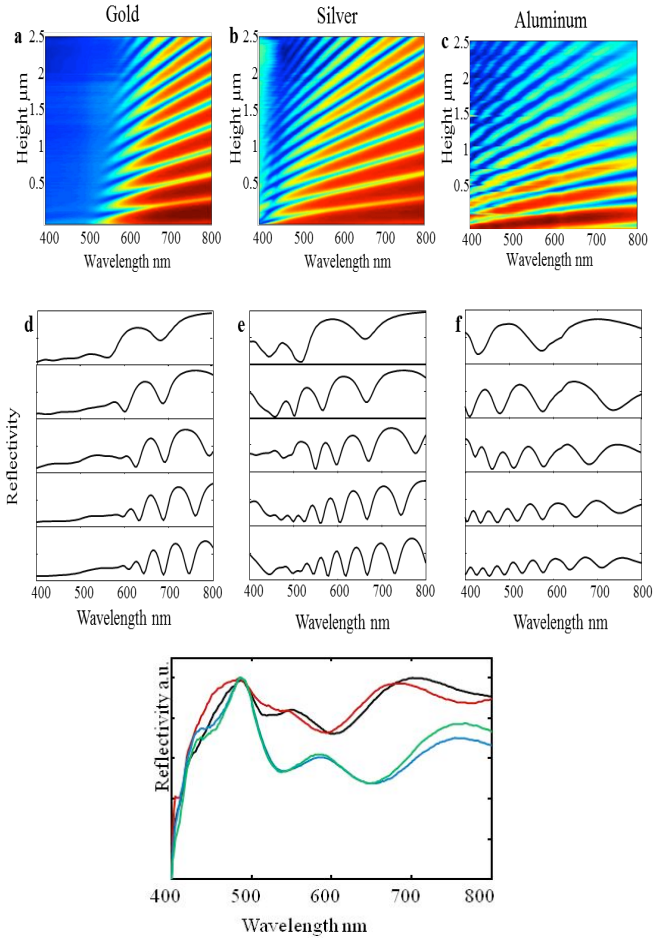

Figure 4. Simulations of the normal incidence reflected power for gold (a), silver (b) and aluminum (c) as a function of wavelength and pillar height. Multiple resonances can be excited bellow the plasmon cutoff frequency. Experimental plots of reflectivity for flat metallic films and arrays of height equal to 0.5, 1, 1.5, and 2 µm for gold (d), silver (e) and aluminum (f). (g) red-shift effect of dielectric. In all plots the reflectivity scale is 0 to 1.

III. CONCLUSIONS AND FUTURE WORK

We demonstrated multiresonant plasmonic nanocavities in vertical metallic nanopillar arrays with strong overlap and coupling between incident light and the plasmon modes. The absorbance of nanostructured metallic surfaces has been engineered to cover multiple wavelengths by increasing the longitudinal dimensions of the plasmon resonant nano-cavities. For large cavity sizes for aluminum and longer for silver and gold, the benefit of multiple resonances is offset by the weaker coupling into plasmons as the round trip

 ISBN: 978-1-61208-214-1

losses in the cavity become significant enough to decrease the electric field amplitude of the modes. Using geometry dependent tuning, the resonances can be further optimized for renewable energy applications for a better overlap with the absorbance of semiconductor materials. Most of the incident light is reflected in the red side of the spectrum, as the resonance spacing is increased at longer wavelengths.

Finally, in terms of application, it needs to be mentioned that the nano-cavities are envisioned for high sensitivity Raman spectroscopy that requires high local electromagnetic fields and alignment between the plasmon resonance and excited and scattered light [18]. Currently, besides Surface Enhanced Raman Spectroscopy which relies on visible resonant structures, we are also extending the cavity resonances to IR as source and detector platforms for enhanced IR spectroscopy. Furthermore, the tunable nanocavity are of particular relevance for fabrication of plasmonic lasers which use surface plasmons instead of light to pump the lasing medium [20], which we are also currently embarking on. Since the device structure relies on vertical free standing nano-pillars the plasmonic cavity region can be filled with any material of choice. Therefore, in addition to the high confinement factors shown, the cavity plasmon resonance can be adjusted for maximum overlap with the absorbance of the active material.

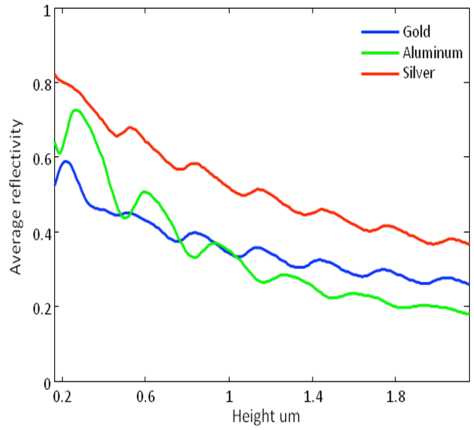

Figure 5. Average absorbance calculated over 400-800nm range.

ACKNOWLEDGMENTS

The authors thank Cindy Larson and Jerry Britten for helping on patterning the samples, Nick Teslich and Ed Sedillio on performing the SEM and/or FIB.. This work was performed under the auspices of the U.S. Department of Energy by Lawrence Livermore National Laboratory under Contract DE-AC52-07NA27344. LLNL- JRNL- 560591.

REFERENCES

[1] Hirsch, L. R., Jackson, J. B., Lee, A., Halas, N. J., and West, J. , Analytical Chemistry , vol. 75, Jan. 2003, , pp. 2377-2381.

[2] Rich, R. L. and Myszka, D. G., Current Opinion in Biotechnology , vol. 11, Oct. 2000 , pp. 54-61.

[3] Bora, M., Celebi, K., Zuniga, J., Watson, C., Milaninia, K. M., and Baldo, M. A., Optics Express, vol. 17, Jul. 2009, pp. 329-336.

[4] Barnes, W. L., Dereux, A., and Ebbesen, T. W., Nature, vol. 424, Jun. 2003 ,pp. 824-830.

[5] Ghaemi, H. F., Thio, T., Grupp, D. E., Ebbesen, T. W. and Lezec, H. J., Physical Review B, vol. 58, Nov. 1998, pp. 6779-6782.

[6] Lezec, H. J., Degiron, A., Devaux, E., Linke, R. A., Martin-Moreno, L., and Garcia-Vidal, F. J.; Ebbesen, T. W., Science, vol. 297, May 2002, pp. 820-823.

[7] Morfa, A. J., Rowlen, K. L., Reilly, T. H., Romero, M. J., and van de Lagemaat, Applied Physics Letters, vol. 92, Aug. 2008, pp. 013504-1-3.

[8] Tvingstedt, K., Persson, N. K., Inganas, O., Rahachou, A.;, and Zozoulenko, I. V., Applied Physics Letters, vol. 91, Mar. 2007, pp. 123514-1-3.

[9] Westphalen, M., Kreibig, U., Rostalski, J., Luth, H., and Meissner, D., Solar Energy Materials and Solar Cells, vol. 61, Jan. 2000, pp. 97-105.

[10] Anker, J. N., et al., Nature Materials, vol. 7, Jul.. 2008, pp. 442-453.

[11] Halas, N.J., Nanoletters, vol. 10, Oct. 2010, pp. 3816-3822.

[12] Zhou, W. and Odom, T., Nature Nanotechnolgy, vol. 6, Jun. 2011, pp. 423-427.

[13] Zhang Z., Weber-Bargioni, A., Wu, S. W., Dhuey, S., Cabrini, S., and Schuck, P.J., Nano Letters, vol. 9, Sept. 2009, pp. 4505-4509.

[14] Zhang J..Z., Optical properties and spectroscopy of nanomaterials, World Scientific Publishers, 2009.

[15] Kubo, N. and Fujikawa S., Nanoletters 2011, 11, pp. 8-15.

[16] Bora, M., et al., Nanoletters, vol. 10, Oct. 2010, pp. 2832-2837.

[17] Fernandez, A., et al., Journal of Vacuum Science Technology B, vol. 15, Apr. 1997, pp. 729-735.

[18] Chang, A. S.-P., et al., unpublished.

[19] Blaber, M.G, Arnold, M.D, and Ford, M. J., Journ Physical Cheminstry C, vol. 113, Dec. 2009, 3041-3046.

[20] Bora, M., et al., unpublished.

 ISBN: 978-1-61208-214-1